Combustion and Flame 156 (2009) 813–825

Contents lists available at ScienceDirect

Combustion and Flame

www.elsevier.com/locate/combustflame

Direct numerical simulation of auto-ignition of a hydrogen vortex ring reacting with hot air

Jeff Doom, Krishnan Mahesh *

Department of Aerospace Engineering and Mechanics, University of Minnesota, 107 Akerman Hall, Minneapolis, MN, United States

ARTICLE INFO

Article history:
Received 25 February 2008
Received in revised form 1 January 2009
Accepted 24 January 2009
Available online 14 February 2009

Keywords:
Reacting
H_2/air
Laminar vortex ring
Auto-ignition

ABSTRACT

Direct numerical simulation (DNS) is used to study chemically reacting, laminar vortex rings. A novel, all-Mach number algorithm developed by Doom et al. [J. Doom, Y. Hou, K. Mahesh, J. Comput. Phys. 226 (2007) 1136–1151] is used. The chemical mechanism is a nine species, nineteen reaction mechanism for H_2/air combustion proposed by Mueller et al. [M.A. Mueller, T.J. Kim, R.A. Yetter, F.L. Dryer, Int. J. Chem. Kinet. 31 (1999) 113–125]. Diluted H_2 at ambient temperature (300 K) is injected into hot air. The simulations study the effect of fuel/air ratios, oxidizer temperature, Lewis number and stroke ratio (ratio of piston stroke length to diameter). Results show that auto-ignition occurs in fuel lean, high temperature regions with low scalar dissipation at a 'most reactive' mixture fraction, ζ_{MR} (Mastorakos et al. [E. Mastorakos, T.A. Baritaud, T.J. Poinsot, Combust. Flame 109 (1997) 198–223]). Subsequent evolution of the flame is not predicted by ζ_{MR}; a most reactive temperature T_{MR} is defined and shown to predict both the initial auto-ignition as well as subsequent evolution. For stroke ratios less than the formation number, ignition in general occurs behind the vortex ring and propagates into the core. At higher oxidizer temperatures, ignition is almost instantaneous and occurs along the entire interface between fuel and oxidizer. For stroke ratios greater than the formation number, ignition initially occurs behind the leading vortex ring, then occurs along the length of the trailing column and propagates toward the ring. Lewis number is seen to affect both the initial ignition as well as subsequent flame evolution significantly. Non-uniform Lewis number simulations provide faster ignition and burnout time but a lower maximum temperature. The fuel rich reacting vortex ring provides the highest maximum temperature and the higher oxidizer temperature provides the fastest ignition time. The fuel lean reacting vortex ring has little effect on the flow and behaves similar to a non-reacting vortex ring.

1. Introduction

The motion of a fluid column of length L through an orifice of diameter D produces a vortex ring. Non-reacting vortex rings have been studied by many researchers, and a large volume of work exists (see e.g. the review by Shariff and Leonard [1]). Less is known about reacting vortex rings. This paper is motivated by the relevance of vortex rings to fuel injection, and uses direct numerical simulation (DNS) to study the flow generated by a piston pushing a ring of gaseous fuel into hot oxidizer.

Past work on non-reacting vortex rings (Maxworthy [2,3]; Didden [4]; Glezer [5]) has studied the process of vortex ring formation, their kinematics, and the temporal evolution of vortex circulation. A notable finding is that of Gharib et al. [6] who show that a vortex ring achieves its maximum circulation at the critical stroke ratio (termed 'formation number') across which the flow transitions from a toroidal vortex ring to a vortex ring with trailing column of vorticity. Here, the stroke length ratio is defined as the ratio of the piston stroke length to the nozzle exit diameter. Sau and Mahesh [7] show how the stroke length affects entrainment and mixing. They show that entrainment is highest at the formation number, and decreases when the trailing column forms. They explain this behavior by showing that a toroidal vortex ring entrains ambient fluid efficiently, but the trailing column does not. As the stroke length increases toward the formation number, the vortex ring remains toroidal, but increases in size and circulation, which increases entrainment. When the stroke ratio exceeds the formation number, the leading vortex ring remains the same, and the trailing column increases in length. The fractional contribution of the leading vortex ring to overall entrainment therefore decreases. Since the trailing column does not entrain ambient fluid efficiently, the overall entrainment drops.

Chen et al. [8–10] have performed experiments on reacting vortex rings of (pure/nitrogen diluted) propane and ethane issuing into air. The fuel and oxidizer are initially at the same temperature (300 K) in their experiments, and a pilot flame is used to initiate combustion. Luminosity measurements are used to provide

* Corresponding author.
E-mail address: mahesh@aem.umn.edu (K. Mahesh).

0010-2180/$ – see front matter
doi:10.1016/j.combustflame.2009.01.010

data on flame shape and height. The fuel volume and ring circulation are varied in a controlled manner. The nozzle exit-velocity is assumed top-hat (U_0), and ring circulation is estimated from hot-wire measurements as $\Gamma = U_0^2 \Delta t$ where Δt is the duration of the pulse. The fuel volume is estimated as $V_F = U_0 \Delta t A$ where A is the nozzle cross-sectional area. Chen et al. also perform simulations of methane/air vortex rings using a steady laminar flamelet approach, where the chemical species and temperature are functions of the conserved scalar and scalar dissipation rate. The speed of the vortex ring is seen to initially increase, and then decrease at later times. Dilatation due to heat release is shown to be responsible for this behavior. The experiments show that as the fuel volume or circulation is changed, the flame structure and burnout time change significantly. The formation number (which they term the overfill limit) does not significantly change from the non-reacting case. Fuel volume which exceeds the overfill limit is seen to decrease heat release and ring speed. Also, the burnout time and flame shapes are quite different for ethane and propane under similar conditions although the stoichiometry and diffusivity are nearly identical. Nitrogen dilution (for propane) decreases burnout time and flame luminosity, but does not appreciably change flame structure.

Simulations of reacting vortex rings in a slightly different configuration were performed by Hewett and Madnia [11] and Safta and Madnia [12]. Hewett and Madnia solved the axisymmetric compressible Navier–Stokes equations and used a one-step Arrhenius mechanism to model combustion of a hydrocarbon in air. No pilot flame exists; instead the vortex ring of fuel issues into hot oxidizer. The stroke ratio of the vortex ring is 2 for all cases considered. The simulations study the effect of oxidizer temperature which is controlled such that ignition occurs either when the vortex rings forms, or occurs after the vortex ring has fully formed. They find that at higher oxidizer temperatures, most of the reaction occurs in front of the vortex ring, while at lower temperatures, most of the reaction occurs inside the ring. The heat released during reaction is shown to affect the ring vorticity and strain rate. Safta and Madnia [12] consider the same problem, but use a methane-hydrogen mixture as fuel. They contrast three chemical mechanisms – GRI-Mech v3.0, and two reduced mechanisms with 11 steps, 15 species and 12 steps, 16 species respectively.

The objective of this paper is to study the coupling between the fluid flow and chemistry with as few simplifying assumptions as possible. We therefore use direct numerical simulation to study the flow when a round nozzle injects $H_2 + N_2$ fuel at room temperature into air at higher temperatures. The amount of fuel injected is controlled by varying the stroke length or stroke ratio. The governing equations are the three-dimensional, unsteady, compressible, Navier–Stokes equations along with conservation equations for the nine species described by the Mueller et al. [13] chemical mechanism. The simulations consider the effects of Lewis number, stroke length ratio and fuel/air mixtures (equivalence ratio) on auto-ignition and the flow.

The auto-ignition behavior is contrasted to the studies of Mastorakos et al. [14] and Echekki and Chen [15]. Mastorakos et al. performed two-dimensional simulation of auto-ignition of laminar and turbulent diffusion flames with one-step chemistry. They found that ignition always occurs at a well-defined mixture fraction (ζ_{MR}). Echekki and Chen [15] used DNS to study auto-ignition of a hydrogen/air mixture in two-dimensional turbulence. Their results showed that there exist spatially localized sites where auto-ignition begins which they define as a "kernel." These kernels occur at high temperatures, fuel-lean mixtures, and low dissipation rates.

The paper is organized as follows. Section 2 describes relevant details of the simulation. It provides a brief description of the governing equations, numerical method, initial and boundary conditions and results from a validation and grid convergence study. The homogeneous mixture problem is discussed in Section 3 and is used to obtain a chemical time scale and ζ_{MR}. Section 4 discusses results for the reacting vortex ring. A brief summary in Section 5 concludes the paper.

2. Simulation details

2.1. Governing equations

The governing equations are the unsteady, compressible, reacting Navier–Stokes equations:

$$\frac{\partial \rho^d}{\partial t^d} + \frac{\partial \rho u_j^d}{\partial x_j^d} = 0,$$

$$\frac{\partial \rho^d Y_k^d}{\partial t^d} + \frac{\partial \rho Y_k^d u_j^d}{\partial x_j^d} = \frac{\partial}{\partial x_j^d}\left(\rho^d D_k^d \frac{\partial Y_k^d}{\partial x_j^d}\right) + \dot{\omega}_k^d,$$

$$\frac{\partial \rho^d u_i^d}{\partial t^d} + \frac{\partial \rho^d u_i^d u_j^d}{\partial x_j^d} = -\frac{\partial p^d}{\partial x_i^d} + \frac{\partial \tau_{ij}^d}{\partial x_j^d},$$

$$\frac{\partial \rho^d E^d}{\partial t^d} + \frac{\partial \left(\rho^d E^d + p^d\right) u_j^d}{\partial x_j^d} = \frac{\partial \tau_{ij}^d u_i^d}{\partial x_j^d} + \frac{\partial}{\partial x_j^d}\left(\mu^d \frac{c_p^d}{Pr} \frac{\partial T^d}{\partial x_j^d}\right) + \sum_{k=1}^{N} Q_k^d \dot{\omega}_k^d,$$

$$p^d = \rho^d R^d T^d = \rho^d \frac{R_u}{W^d} T^d.$$

Here, the superscript 'd' denotes dimensional values. From Doom et al. [16], non-dimensional variables are defined as:

$$\rho = \frac{\rho^d}{\rho_r}, \qquad u_i = \frac{u_i^d}{u_r}, \qquad t = \frac{t^d}{L/u_r},$$

$$\mu = \frac{\mu^d}{\mu_r}, \qquad p = \frac{p^d - p_r}{\rho_r {u_r}^2},$$

$$T = \frac{T^d}{T_r}, \qquad M_r = \frac{u_r}{a_r} = \frac{u_r}{\sqrt{\gamma R_r T_r}}, \qquad p_r = \rho_r R_r T_r,$$

$$Y_k = \frac{Y_k^d}{Y_r}, \qquad D_k = \frac{D_k^d}{u_r L}, \qquad \dot{\omega}_k = \frac{L \dot{\omega}_k^d}{u_r \rho_r Y_r},$$

$$Q_k = \frac{Y_r Q_k^d}{c_{p,r} T_r}, \qquad R_r = \frac{R_u}{W_r}, \quad \text{and} \quad W = \frac{W^d}{W_r}.$$

Here, the subscript 'r' denotes reference variables. This yields the following non-dimensional governing equations:

$$\frac{\partial \rho}{\partial t} + \frac{\partial \rho u_j}{\partial x_j} = 0,$$

$$\frac{\partial \rho Y_k}{\partial t} + \frac{\partial \rho Y_k u_j}{\partial x_j} = \frac{1}{Re\, Sc_k} \frac{\partial}{\partial x_j}\left(\mu \frac{\partial Y_k}{\partial x_j}\right) + \dot{\omega}_k,$$

$$\frac{\partial \rho u_i}{\partial t} + \frac{\partial \rho u_i u_j}{\partial x_j} = -\frac{\partial p}{\partial x_i} + \frac{1}{Re} \frac{\partial \tau_{ij}}{\partial x_j},$$

$$M_r^2 \left[\frac{\partial}{\partial t}\left(p + \frac{\gamma - 1}{2} \rho u_i u_i\right) + \frac{\partial}{\partial x_j}\left(\gamma p + \frac{\gamma - 1}{2} \rho u_i u_i\right) u_j\right] + \frac{\partial u_j}{\partial x_j} = \frac{(\gamma - 1) M_r^2}{Re} \frac{\partial \tau_{ij} u_i}{\partial x_j} + \frac{1}{Re\, Pr} \frac{\partial}{\partial x_j}\left(\frac{\mu}{W} \frac{\partial T}{\partial x_j}\right) + \underbrace{\sum_{k=1}^{N} Q_k \dot{\omega}_k}_{\dot{\omega}_n},$$

$$\frac{\rho T}{W} = \gamma M_r^2 p + 1.$$

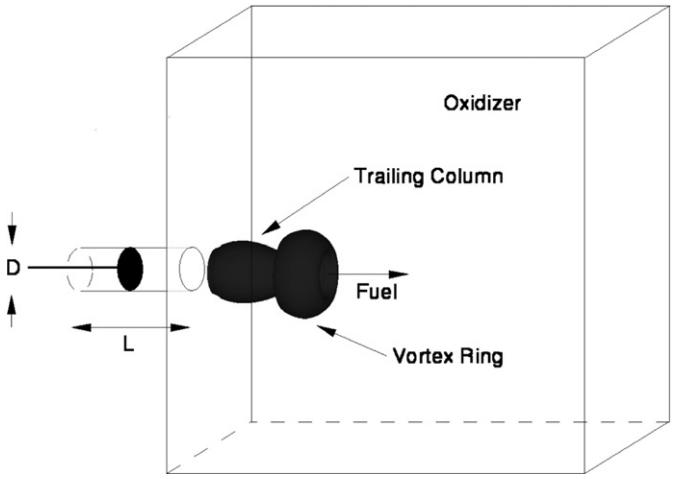

Fig. 1. Schematic of the problem.

The viscous stress tensor is defined as $\tau_{ij} = \mu\left(\frac{\partial u_i}{\partial x_j} + \frac{\partial u_j}{\partial x_i} - \frac{2}{3}\frac{\partial u_k}{\partial x_k}\delta_{ij}\right)$. The source term is denoted as $\dot{\omega}_k$ which is modeled using the Arrhenius law. The heat of reaction per unit mass in the energy equation is Q_k and $\sum Q_k\dot{\omega}_k$ or $\dot{\omega}_n$ is the heat release due to chemical reaction. Sc_k is the Schmidt number for the kth species, Pr is the Prandtl number, Re is the Reynolds number and W is the mean molecular weight of the mixture.

2.2. Numerical method

Note that (Doom et al. [16]) the Navier–Stokes equations are non-dimensionalized using an incompressible scaling for pressure, i.e. $p = \frac{p^d - p_r}{\rho_r u_r^2}$. The energy equation is then interpreted as an equation for the divergence of velocity. Note that when the reference Mach number (M_r) is zero, the non-dimensional divergence of velocity equals the sum of the terms involving thermal conduction and heat release. If the density is constant and there is no heat release, the energy equation reduces to the incompressible continuity equation. In the presence of heat release, the zero Mach number reacting equations (Majda and Sethian [17]) are obtained.

The numerical algorithm is discussed in detail by Doom et al. [16]. The algorithm is fully implicit, spatially non-dissipative and second order in time and space. The thermodynamic variables and species are staggered in time from velocity. All variables are co-located in space. A pressure-correction method is used to enforce velocity divergence obtained from the energy equation. The discrete equations discretely conserve kinetic energy in the incompressible, non-reacting, inviscid limit. These features make the algorithm stable and accurate at high Reynolds numbers, and efficient at both low and finite Mach numbers.

2.3. Problem statement

Fig. 1 shows a schematic of the problem and illustrates the ring vortex and the trailing column which forms at large stroke ratios. The dimensional variables for the reacting vortex ring are chosen such that the equivalence ratio (ϕ) is one, and a stoichiometric mixture is obtained where $Y_{H_2,0}$ equals 0.02936 and $Y_{O_2,0}$ equals 0.233. For fuel lean mixtures, ϕ equals 0.25 ($Y_{H_2} = 0.0074$) and for fuel rich mixtures ϕ equals 4 ($Y_{H_2} = 0.1185$). For all simulations, Re is 1000, Pr is 0.7 and μ is equal to $T^{0.7}$. The non-uniform Lewis numbers are [18]:

$$Le_{H_2} = 0.3, \quad Le_{O_2} = 1.11, \quad Le_O = 0.7, \quad Le_{OH} = 0.73, \quad (1)$$
$$Le_{H_2O} = 0.83, \quad Le_H = 0.18, \quad Le_{HO_2} = 1.10,$$

Table 1
Inlet boundary conditions.

Non-dimensional inlet variables	
T_{in}	$(T_O - T_F)\left(1 - \left[\frac{1}{2} - \frac{1}{2}\tanh(10[\sqrt{y^2+z^2} - 1])\right]\right) + T_F$
u_{in}	$u_F\left(\frac{1}{2} - \frac{1}{2}\tanh[10(\sqrt{y^2+z^2} - 1)]\right)U_{time}$
$Y_{H_2,in}$	$Y_{F_0}\left(\frac{1}{2} - \frac{1}{2}\tanh[10(\sqrt{y^2+z^2} - 1)]\right)U_{time}$
$Y_{O_2,in}$	$Y_{O_0}\left(1 - \left[\frac{1}{2} - \frac{1}{2}\tanh(10[\sqrt{y^2+z^2} - 1])\right]\right)$
p_{in}	0
ρ_{in}	$\frac{MW_{in}}{T_{in}}$

$$Le_{H_2O_2} = 1.12, \quad (2)$$

where $Le_k = \frac{Sc_k}{Pr}$. Reference pressure, length, Mach number and time are 1.0132e5 Pa, 0.01 m, 0.4, and 6.6e−5 s, respectively.

The inflow boundary conditions are shown in Table 1. T_O and T_F denote the oxidizer and fuel temperatures respectively. u_F is the fuel velocity at the nozzle exit. Y_{F_0} and Y_{O_0} denote the mass fractions of fuel and oxidizer, respectively. U_{time} controls the stroke length (L/D). Note that all reference variables are non-dimensionalized with respect to the fuel side. The first derivative is set to zero for thermodynamic variables, species, and velocities at the outflow. At the y and z boundaries, the thermodynamic variables and species are set to a constant (same as initial conditions) and the velocities are set to zero. 'Sponge' boundary conditions (Colonius et al. [19]) are used at the outflow and transverse boundaries to absorb acoustic waves that are generated by the flame. A cooling term, $-\sigma(U - U_{ref})$, is added to the right hand side of the governing equations over the sponge zone whose length is 10 percent of the domain. Here U and U_{ref} denote the vector of conservative variables and the 'reference' solution, respectively. The coefficient σ for the sponge at the outflow, is a polynomial function defined as:

$$\sigma(x) = A_s\frac{(x - x_s)^n}{(L_x - x_s)^n},$$

where x_s and L_x denotes the start of the sponge and the length of the domain. n and A_s are equal to three.

2.4. Validation and grid-convergence study

The simulations are first validated using a one-step chemical mechanism, and compared to the one-step simulations of Hewett and Madnia [11]. Our results are compared to case 5 in their paper where the temperature ratio is 6:1 and the stroke length is two. Fig. 2(a) shows that good agreement is obtained.

Next, complex chemistry is validated using the homogeneous mixture or well-stirred reactor problem. We use the 9 species (H_2, O_2, OH, O, H, H_2O, HO_2, H_2O_2, and N_2), 19 reaction Mueller mechanism (Mueller et al. [13]) which is shown in Table 2. A detailed experiment and simulation of a laminar hydrogen jet diffusion flame was performed by Cheng et al. [20]. Their work shows that chemical mechanisms from Miller and Bowman [21], GRI-Mech 3.0 [22], Mueller et al. [13], Maas and Warnatz [23], and O'Conaire et al. [24] compare well with experimental results. Therefore, the Mueller mechanism should perform adequately for our hydrogen/air reacting vortex ring simulation. Fig. 2(b) is a comparison between Chemkin [25] and our algorithm incorporating the Mueller mechanism. Good agreement is observed for the homogeneous mixture.

The three-dimensional computational grid used in the simulations is based on a grid refinement study of a two-dimensional H_2/air reacting vortex ring. The computational domain was 10 by 10 in x and y where the nozzle is in the y direction. Uniform grids ranging from 64 to 512 points were used to obtain a grid-converged solution. Also, a non-uniform grid of 128 points in the

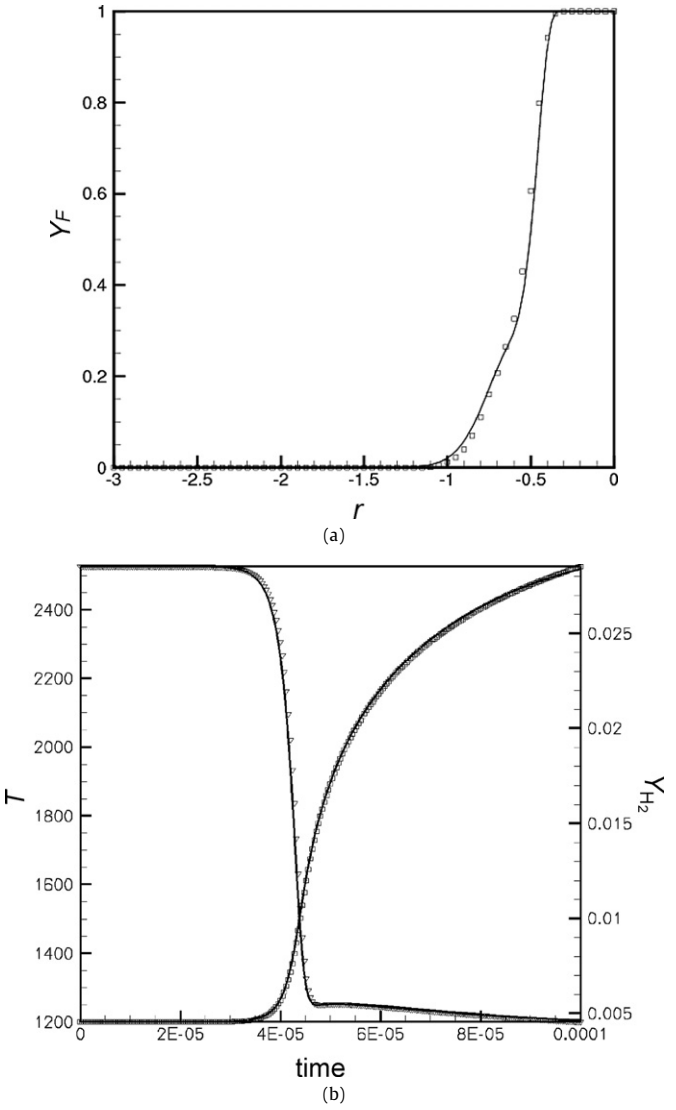

Fig. 2. (a) Comparison using one-step chemistry to Hewett and Madnia [11]. (—) Present, (□) Hewett and Madnia. (b) Comparison of a major species and temperature between Chemkin and present algorithm for a well-stirred reactor using the Mueller mechanism. Y_{H_2}: (—) Algorithm, (▽) Chemkin and T: (– – –) algorithm, (□) Chemkin.

y direction (to cluster points around the nozzle) and 128 uniform points in the x direction was used. Figs. 3(a) and 3(b) show profiles in the middle of the reacting vortex ring. Note that grid convergence is obtained for the non-uniform grid of 128^2 and uniform 256^2 and 512^2 grids. To ensure adequate resolution for the three-dimensional reacting vortex ring, a non-uniform 128 grid in y, z directions and 256 in the x direction was chosen, and the size of the computational domain was 10 by 10 by 10 in the three coordinate directions.

3. Homogeneous problem

We first consider the homogeneous mixture or well-stirred reactor problem. Our objectives are to: (1) obtain an ignition time scale; (2) obtain an optimum mixture fraction for auto-ignition (Mastorakos et al. [14]); (3) identify which reactions contribute to auto-ignition and which reactions contribute after auto-ignition. Echekki and Chen [15] used DNS to study auto-ignition of a hydrogen/air mixture in two-dimensional turbulence. They found that the intermediate species O, H, OH, and HO_2 play an important role

Table 2
Mueller mechanism ($A_f j$, β_j, and E_j are in cm^3, mol, s, kcal, K).

		A_{fj}	β_j	E_j
	H_2/O_2 chain reactions			
1	$H + O_2 \rightleftharpoons O + OH$	1.910E14	0.0	16.44
2	$O + H_2 \rightleftharpoons H + OH$	5.080E04	2.67	6.29
3	$H_2 + OH \rightleftharpoons H_2O + H$	2.160E08	1.51	3.43
4	$O + H_2O \rightleftharpoons OH + OH$	2.970E06	2.02	13.4
	H_2/O_2 dissociation/recombination reactions			
5	$H_2 + M \rightleftharpoons H + H + M$	4.580E19	−1.40	104.38
6	$O + O + M \rightleftharpoons O_2 + M$	6.160E15	−0.5	0
7	$O + H + M \rightleftharpoons OH + M$	4.710E18	−1.0	0
8	$H + OH + M \rightleftharpoons H_2O + M$	2.210E22	−2.0	0
	Formation and consumption of HO_2			
9	$H + O_2 + M \rightleftharpoons HO_2 + M$	3.50E16	−0.41	−1.12
10	$HO_2 + H \rightleftharpoons H_2 + O_2$	1.660E13	0.0	0.82
11	$HO_2 + H \rightleftharpoons OH + OH$	7.080E13	0.0	0.3
12	$HO_2 + O \rightleftharpoons OH + O_2$	3.250E13	0.0	0
13	$HO_2 + OH \rightleftharpoons H_2O + O_2$	2.890E13	0.0	−0.50
	Formation and consumption of H_2O_2			
14	$HO_2 + HO_2 \rightleftharpoons H_2O_2 + O_2$	4.200E14	0.0	11.98
15	$H_2O_2 + M \rightleftharpoons OH + OH + M$	1.20E17	0.0	45.5
16	$H_2O_2 + H \rightleftharpoons H_2O + OH$	2.410E13	0.0	3.97
17	$H_2O_2 + H \rightleftharpoons H_2 + HO_2$	4.820E13	0.0	7.95
18	$H_2O_2 + O \rightleftharpoons OH + HO_2$	9.550E06	2.0	3.97
19	$H_2O_2 + OH \rightleftharpoons H_2O + HO_2$	1.000E12	0.0	0

in the auto-ignition process. In the Mueller mechanism, reactions 1, 2, 3, 9, 10 and 11 have a significant contribution to the minor species O, H, OH, and HO_2. Fig. 4(a) shows reaction rates of species H due to reactions 1, 2, 3, 9, 10 and 11. Fig. 4(b) shows temperature and heat release when all the reactions are simulated, and when only the auto-ignition reaction (1, 2, 3, 9, 10, and 11) are simulated. Note that the maximum heat release for the full reaction set and the auto-ignition reaction set occurs at about the same time. Up until this instant of maximum heat release, the auto-ignition reactions are dominant; after this instant, the other reactions are also significant. This instant is defined as τ_{chem} and will be used to obtain the most reactive mixture fraction, ζ_{MR}.

Mastorakos et al. [14] used one-step chemistry and the homogeneous mixture problem to obtain τ_{chem} and the mixture fraction most likely to auto-ignite (ζ_{MR}). The following equations are used to set up the well-stirred reactor problem in terms of the mixture fraction defined as:

$$Y_{H_2} = Y_{H_2,0}\zeta, \qquad Y_{O_2} = Y_{O_2,0}(1-\zeta),$$
$$Y_{N_2} = 1 - Y_{H_2} - Y_{O_2}, \qquad T = T_O - \zeta(T_O - T_F). \tag{3}$$

For example, if $\zeta = 0.5$, $Y_{H_2,0} = 0.029$, $Y_{O_2,0} = 0.233$, $T_F = 300$ (K) and $T_O = 1200$ (K), then Y_{H_2}, Y_{O_2}, Y_{N_2}, and T would be 0.0145, 0.1165, 0.869, and 750 (K), respectively. One can now consider different initial mixture fractions, obtain the minimum ignition time (τ_{chem}) and thereby obtain the most reactive mixture fraction (ζ_{MR}).

We obtain ζ_{MR} for the Mueller mechanism. Fig. 5(a) shows mixture fraction versus τ_{chem} for initial temperatures that range from 1100 to 1400 K and Fig. 5(b) shows mixture fraction versus τ_{chem} for fuel/air ratios (ϕ) that range from 0.25 to 8. Note in Fig. 5 that the minimum τ_{chem} corresponds to ζ_{MR}. Fig. 5 also shows the effect of fuel/air mixture and temperature on τ_{chem}. As temperature increases, τ_{chem} becomes smaller and ζ_{MR} shifts to the right. As ϕ increases, τ_{chem} becomes smaller and ζ_{MR} shifts to the left. These results illustrate the balance between adequate fuel and high enough temperature for auto-ignition to occur. Table 3 lists the most reactive mixture fraction and corresponding values of the initial temperature, fuel/air ratio and τ_{chem}.

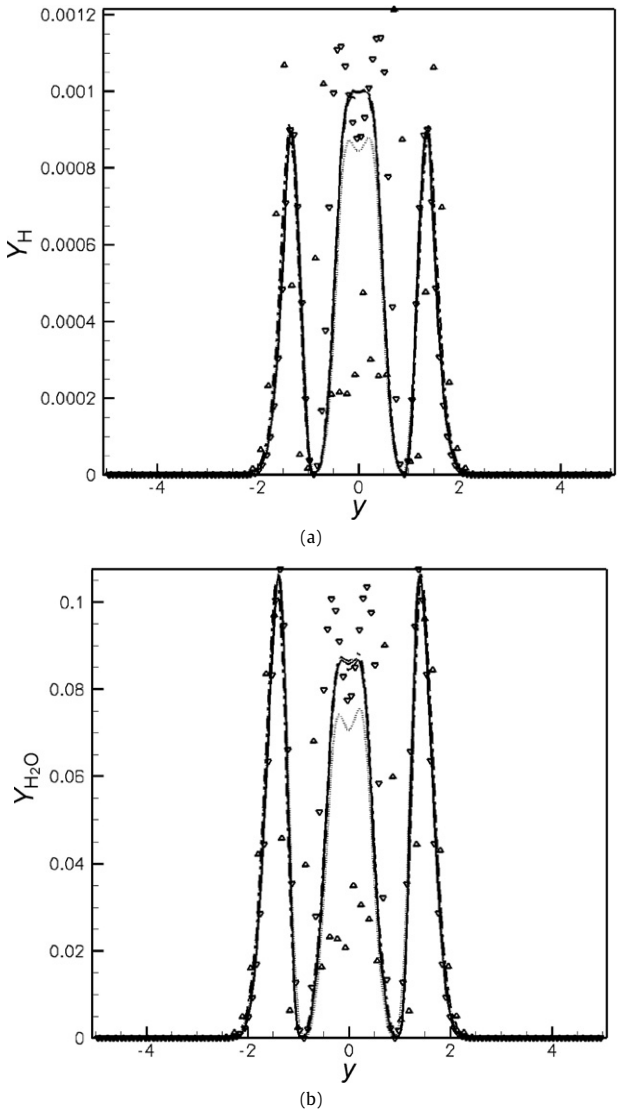

Fig. 3. Grid convergence study for a two–dimensional laminar reacting vortex ring. (a) Y_H, (b) Y_{H_2O}. ($\triangle$) $N = 64$, ($\triangledown$) $N = 128$, ($\cdots$) $Nx = 128$, $Ny = Nz = 128$ non-uniform in y, ($---$) $Nx = 256$, $Ny = Nz = 128$ non-uniform in y, ($--$) $N = 256$, ($-$) $N = 512$.

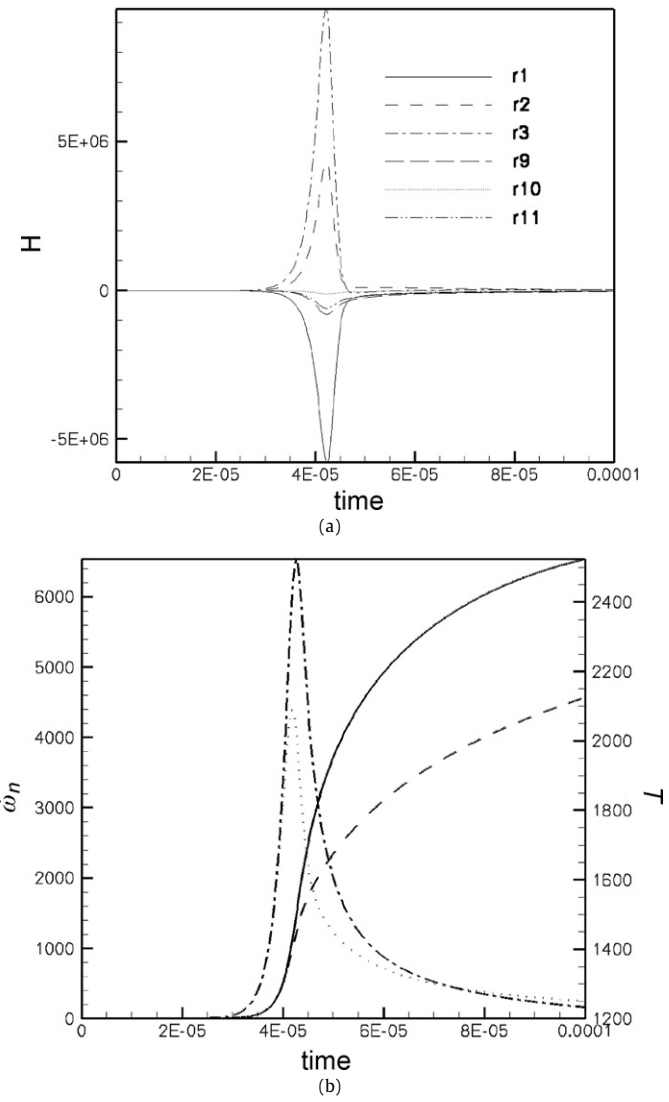

Fig. 4. (a) Rates of reactions 1, 2, 3, 9, 10 and 11 for species H. (b) Temporal evolution of temperature with all reactions, and reactions 1, 2, 3, 9, 10 and 11. All reactions: T ($-$), $\dot{\omega}_n$ ($---$); reactions 1, 2, 3, 9, 10 and 11: T ($--$), $\dot{\omega}_n$ ($\cdots$).

4. Results for reacting vortex ring

Table 4 lists the different cases studied. The simulations consider the effect of Lewis number, stroke length ratio (L/D), fuel/air ratio and oxidizer temperature. The non-uniform Lewis numbers are obtained from Im et al. [18]. Two stroke ratios of 2 and 6 are considered. Note that for non-reacting vortex rings, a stroke ratio of 2 yields a coherent vortex ring, while a stroke ratio of 6 yields a vortex ring followed by a trailing column of vorticity (Sau and Mahesh [7]). Oxidizer temperatures (T_O) of 1200 and 1800 K are considered. Finally, fuel/air ratios were chosen such that the equivalence ratios (ϕ) are equal to 1/4, 1 and 4 yielding lean, stoichiometric and rich mixtures, respectively.

4.1. Ignition and flame evolution

We first consider the non-uniform Lewis number simulations at stroke ratio of 2 and oxidizer temperature of 1200 K. Fig. 6 shows reactions 1, 2, 3, 9, 10 and 11 for the species H. Time is normalized by τ_{chem} obtained from Table 3. Comparison to a corresponding plot for the homogeneous mixture (Fig. 4(a)) shows qualitative similarities along with some differences. The reaction rates are seen to peak at time greater than τ_{chem} for the reacting vortex ring, reflecting the finite amount of time taken for fuel and oxidizer to be advected and then diffuse to yield regions of ζ_{MR}. Also, the relative importance of reactions 9 and 11 is higher for the vortex ring. The time scale on which the reaction rates decay to zero following the initial ignition, is longer for the reacting vortex ring, reflecting the propagation of the flame through the vortex ring.

Fig. 7 illustrates the process of auto-ignition in the vortex ring using scatter plots of mixture fraction versus heat release at different instances in time. At each time instant, heat release contours in a radial cross-section are shown. Superposed on the heat release contours is a colored contour line of mixture fraction (ζ), temperature (T) and scalar dissipation (χ), respectively. Note that the color contours of heat release ($\dot{\omega}_n$) range from 0 to 1. Mixture fraction and scalar dissipation are defined as (Poinsot and Veynante [26]):

$$\zeta = \left(\frac{1}{1+\phi}\right)\left(\phi\frac{Y_F}{Y_F^0} - \frac{Y_O}{Y_O^0} + 1\right), \tag{4}$$

$$\chi = \frac{2}{Re}\left(\frac{\partial\zeta}{\partial x_j}\frac{\partial\zeta}{\partial x_j}\right), \tag{5}$$

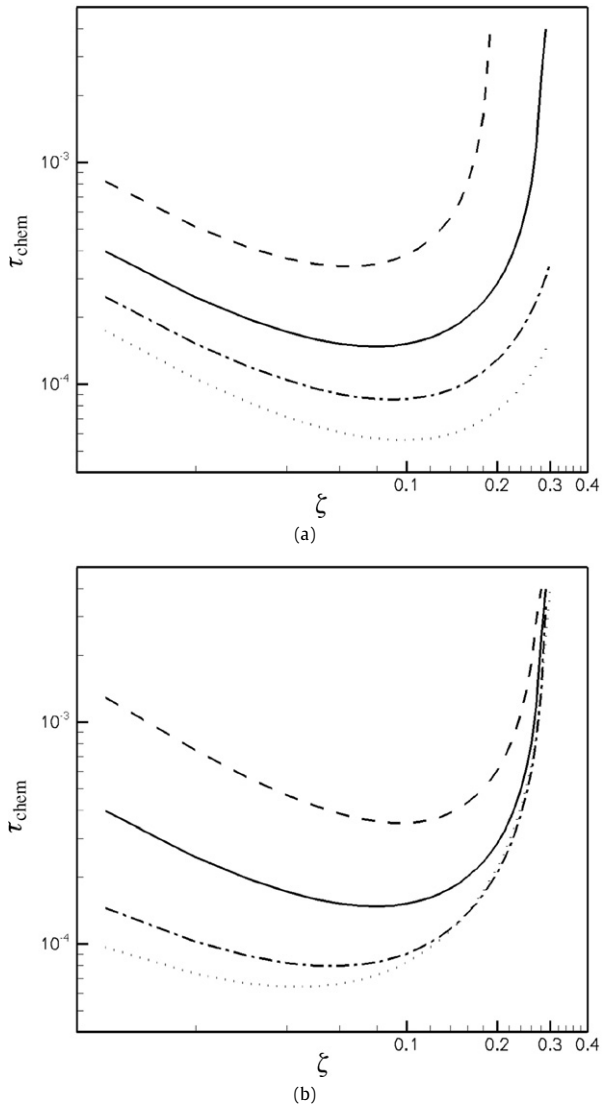

Fig. 5. (a) Mixture fraction versus τ_{chem} for varying temperature in Kelvin. (– – –) $\phi = 1$, $T = 1100$, (—) $\phi = 1$, $T = 1200$, (— – —) $\phi = 1$, $T = 1300$, and (···) $\phi = 1$, $T = 1400$. (b) Mixture fraction versus τ_{chem} for varying fuel/air ratio (– – –) $\phi = 1/4$, $T = 1200$, (—) $\phi = 1$, $T = 1200$, (— – —) $\phi = 4$, $T = 1200$, and (···) $\phi = 8$, $T = 1200$.

Table 3
Global results for homogeneous mixture problem.

T (K)	ϕ	ζ_{MR}	τ_{chem} (s)	T_{MR} (K)
1100	1	0.06	3.4e−4	1052
1200	1	0.08	1.4e−4	1128
1300	1	0.09	8.5e−5	1210
1400	1	0.10	5.6e−5	1290
1800	1	0.13	1.8e−5	1605
1200	1/4	0.1	3.5e−4	1110
1200	4	0.06	8.0e−5	1146
1200	8	0.04	6.4e−5	1164

respectively. For the contour lines, mixture fraction is purple (contour lines range from 0.04 to 0.12), temperature is black (contour lines range from 1120 to 1140 K) and scalar dissipation is red (contour lines vary over the entire range of 0.0 to 0.15). Note that the ranges for the contour lines of mixture fraction and temperature were chosen based on the results of the homogeneous mixture problem. Recall ζ_{MR} is 0.08 from the homogeneous problem when $T_0 = 1200$ K and $\phi = 1$ (Table 3).

Fig. 7 shows that auto-ignition occurs in regions of high temperature, fuel-lean mixtures, and low scalar dissipation where $\zeta = \zeta_{MR}$. Ignition occurs at a ζ_{MR} of 0.08 and propagates toward the stoichiometric side ($\zeta = 0.5$). Most of the ignition occurs behind the vortex ring and then moves rapidly into the core. The contour line of mixture fraction shows that auto-ignition occurs in fuel lean regions ($\zeta = \zeta_{MR} = 0.08$). Also, the contour lines of scalar dissipation show that auto-ignition occurs in regions of low scalar dissipation.

Table 4
Parameters used in reacting vortex ring simulations.

Lewis number	ϕ	(L/D)	T_O
Non-uniform	1	2	1200
Unity	1	2	1200
Non-uniform	0.25	2	1200
Non-uniform	4	2	1200
Non-uniform	1	2	1800
Non-uniform	1	6	1200

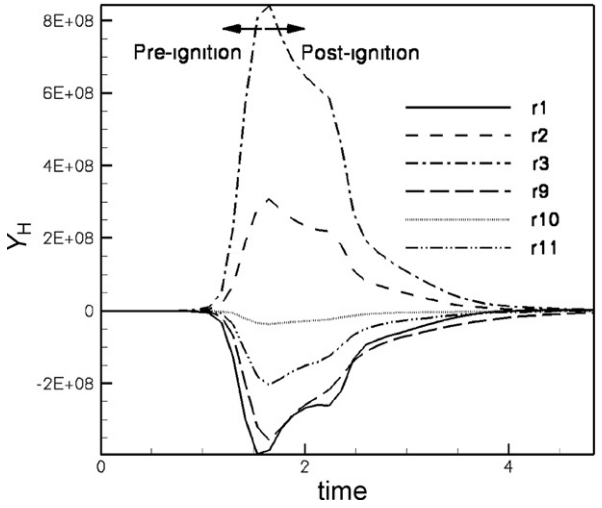

Fig. 6. Domain average of rates of reactions 1, 2, 3, 9, 10 and 11 for the species H. Non-uniform Lewis (—) reaction 1, (– – –) reaction 2, (— – —) reaction 3, (— — —) reaction 9, (···) reaction 10, (—·· —) reaction 11.

The superposed contour lines of temperature are chosen to lie around T_{MR} which is 1130 K ($T_{MR} = 1200 - \zeta_{MR}[1200 - 300]$). Interestingly, maximum heat release follows T_{MR} at every instant of time in Fig. 7. Fig. 8 is a side by side comparison of ζ_{MR} and T_{MR}. This figure shows that the onset of ignition occurs at ζ_{MR} and T_{MR}. As ignition continues from behind the vortex ring into the core, ζ_{MR} is in the very fuel lean region and does not follow the path of ignition. T_{MR} on the other hand, follows the path of ignition all the way into the core. This suggests that T_{MR} instead of ζ_{MR} might be better in predicting the evolution of auto-ignition. This behavior is observed in all cases simulated (Fig. 8); i.e. in the pre-ignition phase, ζ_{MR} predicts the onset of ignition fairly well, however T_{MR} predicts both the onset of ignition as well as its subsequent evolution.

Table 5 lists most reactive mixture fraction, burnout time in seconds, maximum temperature in Kelvin and ignition time in seconds obtained from all the simulations. Note that the onset of ignition largely depends on fuel/air ratio and oxidizer temperature. However, in the post-ignition phase, the evolution of the flame is greatly affected by other parameters. This behavior is discussed in the following sections.

4.2. Evolution of heat release

Fig. 9 shows the effects of Lewis number, fuel/air ratio, oxidizer temperature and stroke ratio on heat release. An ignition delay is noticeable for all cases except the higher oxidizer temperature

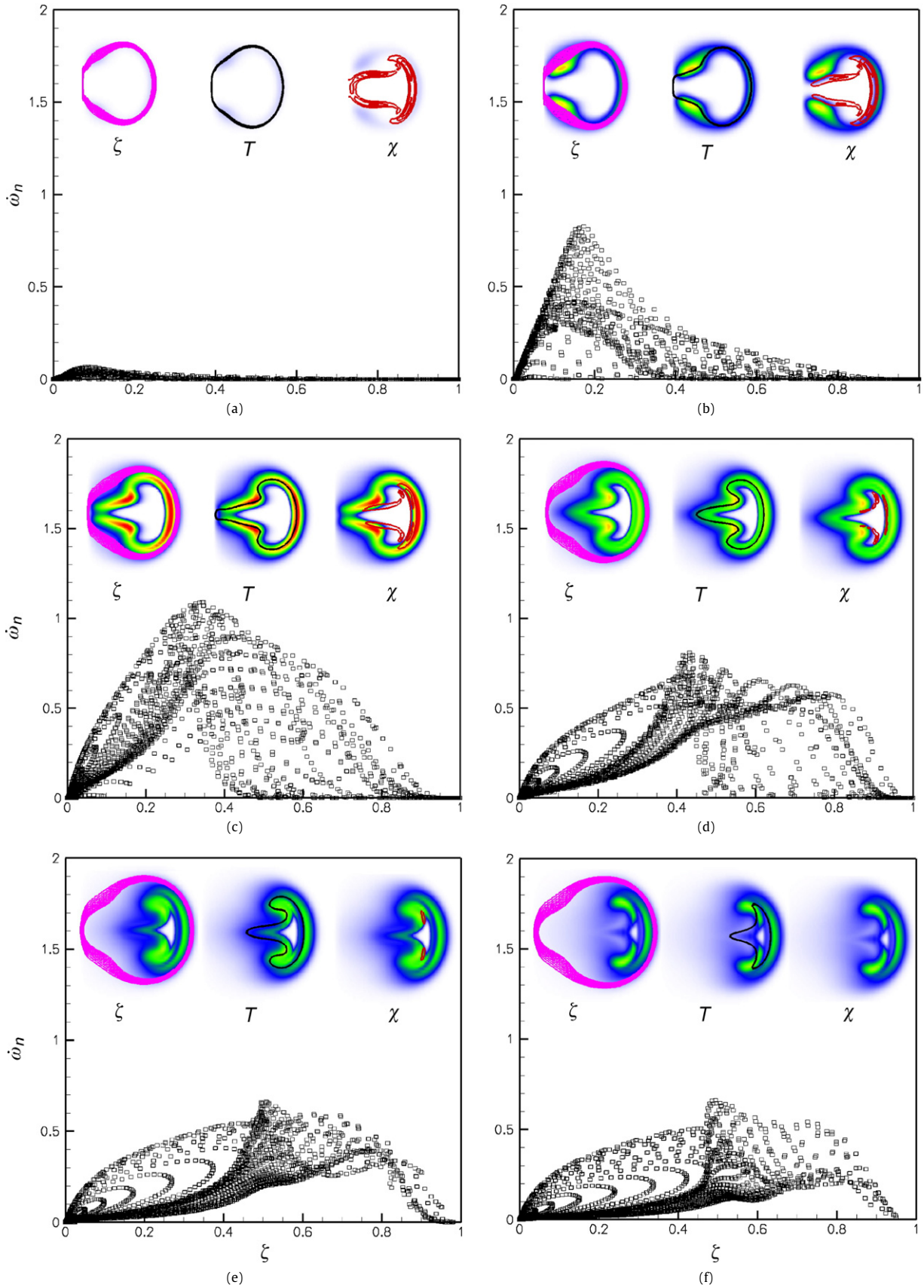

Fig. 7. Two-dimensional slices showing variation in time of ζ versus $\dot{\omega}_n$. The color contours correspond to $\dot{\omega}_n$. On each color contour, a colored contour line is plotted for ζ, T and χ. The color contour of $\dot{\omega}_n$ ranges from 0 to 1. For the contour lines, purple is ζ (contour lines range from 0.04 to 0.12), T is black (contour lines range from 1120 to 1140 K) and χ is red (contour lines range from 0.0 to 0.15). Non–dimensional time: (a) 2.5, (b) 3.0, (c) 3.5, (d) 4.0, (e) 4.5 and (f) 5.0. (For interpretation of the references to color in this figure legend, the reader is referred to the web version of this article.)

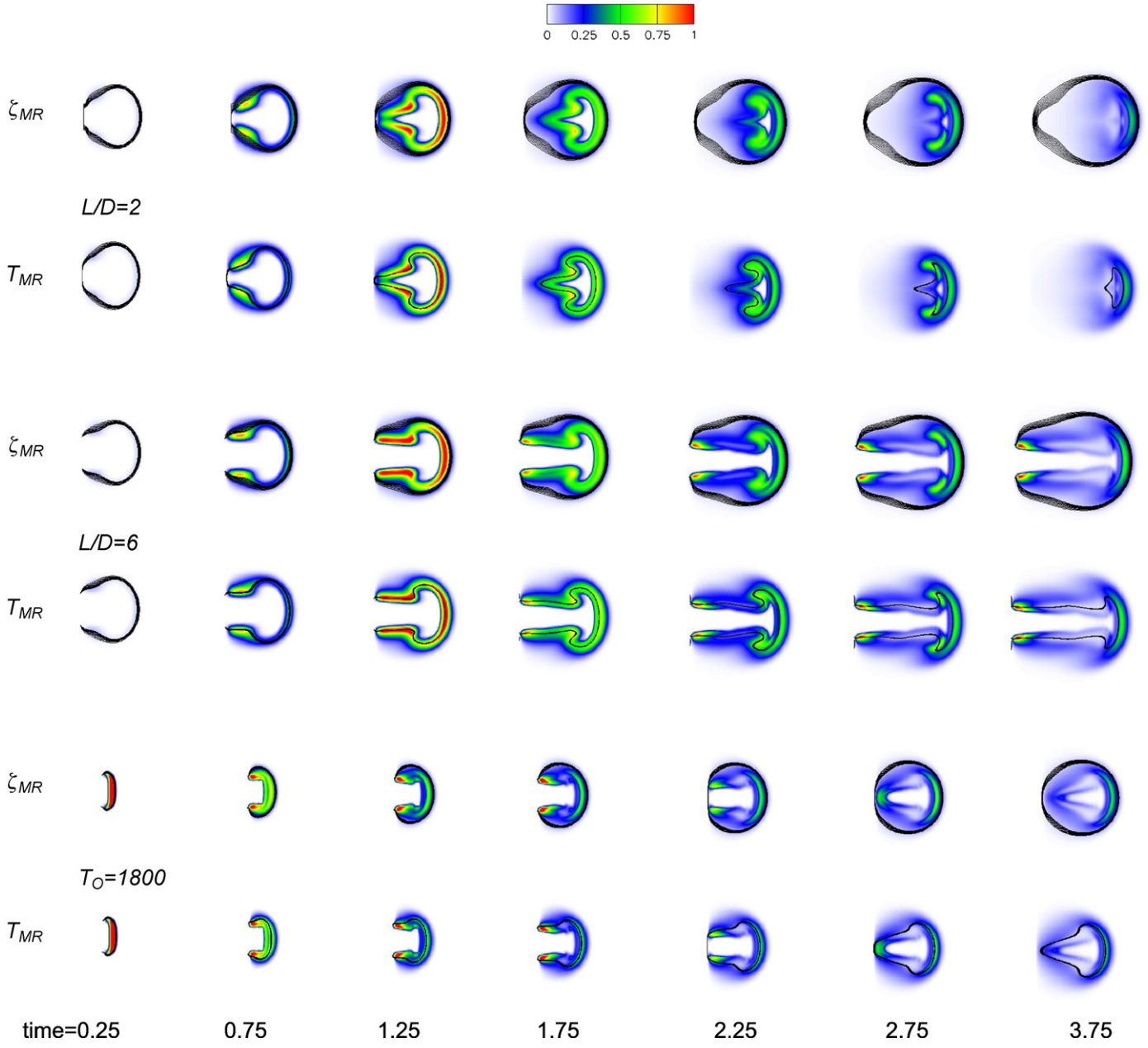

Fig. 8. Time evolution of heat release ($\dot{\omega}_n$), ζ_{MR} and T_{MR}. On each color contour of heat release, a contour line is superimposed for ζ and T. The contour of $\dot{\omega}_n$ ranges from 0 to 1. The contour lines of ζ range from 0.04 to 0.12 (ζ_{MR}) and temperature ranges from 1092 to 1164 K (T_{MR}) for $L/D = 2$ and $L/D = 6$. For oxidizer temperature of 1800 K, ζ ranges from 0.10 to 0.18 (ζ_{MR}) and temperature ranges from 1590 to 1650 K (T_{MR}). (For interpretation of the references to color in this figure legend, the reader is referred to the web version of this article.)

Table 5
Global behavior of the reacting vortex rings.

ϕ	Le_k	1200	L/D	ζ_{MR}	Burnout (s)	T_{max} (K)	Ignition time
1	$Le_k \neq 1$	1200	2	0.08	5.6e−4	1887	1.7e−4
1	$Le_k = 1$	1200	2	0.08	7.1e−4	2105	2.3e−4
1/4	$Le_k \neq 1$	1200	2	0.1	7.4e−4	1227	2.8e−4
4	$Le_k \neq 1$	1200	2	0.055	5.5e−4	2890	1.3e−4
1	$Le_k \neq 1$	1800	2	0.14	5.0e−4	2263	1.7e−5
1	$Le_k \neq 1$	1200	6	0.09	1.0e−3	2054	1.7e−4

simulation. The ignition times for all cases are listed in Table 5. For non-uniform and uniform Lewis number at stroke ratio of 2 (Figs. 9(a) and 9(b)), ignition occurs behind the vortex ring, and then propagates rapidly into the core. Note that the heat release for the non-uniform Lewis number simulation is clearly different from that obtained using unity Lewis number. At non-uniform Lewis numbers, the lighter fuel diffuses faster toward the oxidizer, thereby decreasing ignition time.

It is interesting to examine why auto-ignition occurs behind the vortex ring. Fig. 10 shows velocity vectors in a radial cross-section superposed on contours of mixture fraction. Note that the ring entrains oxidizer in the rear; the region of ζ_{MR} is therefore 'thicker' behind the vortex ring compared to the front. Since the global Damköhler number is low ($Da = \frac{\tau_r}{\tau_{chem}} = \frac{6.6e-5}{1.4e-4} = 4.7e{-}01$), the effects of this entrainment will be felt on the time-scale of the chemistry. Auto-ignition therefore occurs behind the ring in this region where ζ_{MR} covers a larger area. Fig. 10 also shows the effects of Lewis number. Note that the regions of ζ_{MR} in the non-

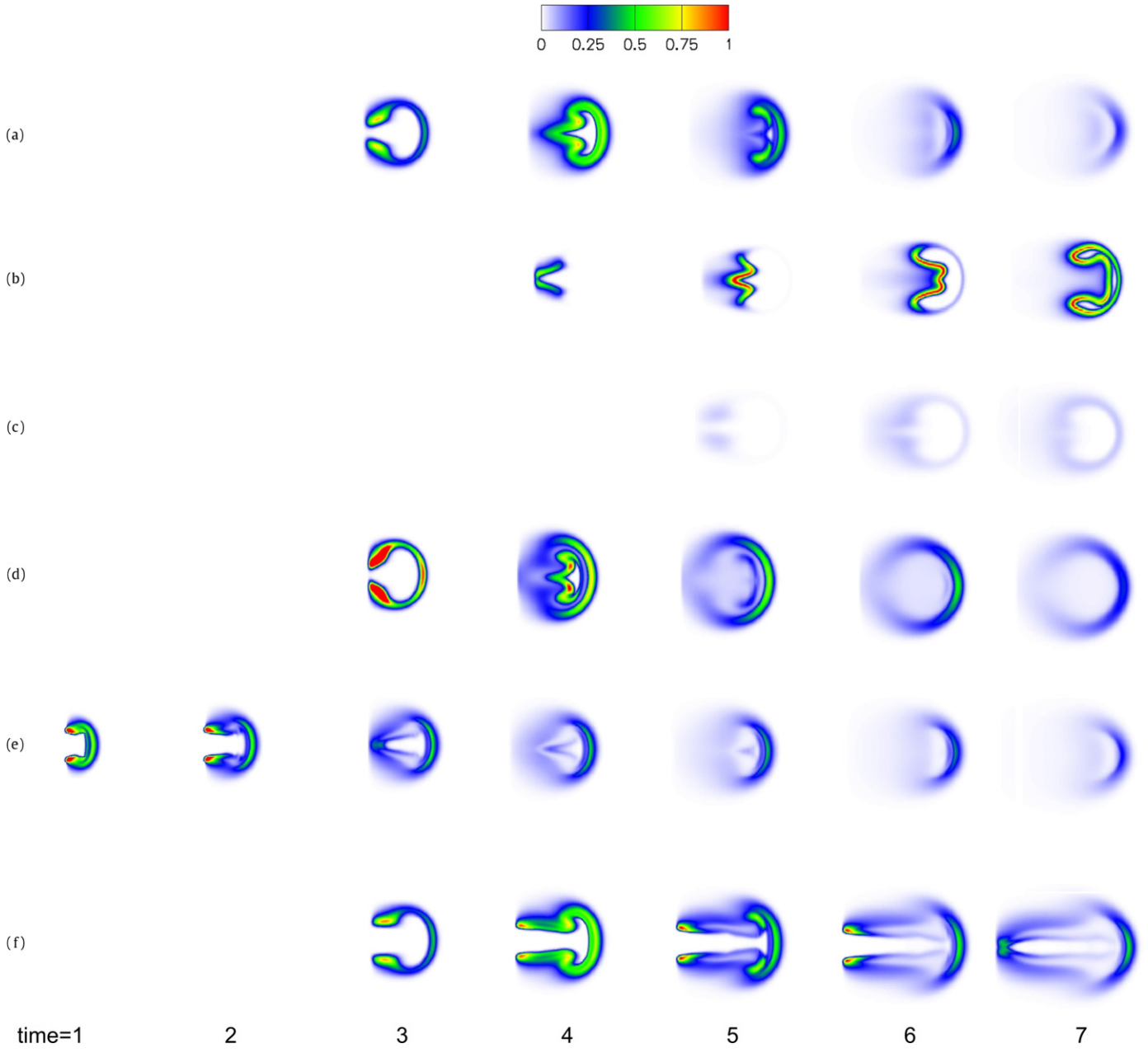

Fig. 9. Time evolution of heat release ($\dot{\omega}_n$). The contours are separated by one unit of time for a total of seven units of time. (a) Non-uniform Lewis number at L/D of 2 and ϕ of 1, (b) uniform Lewis number at L/D of 2 and ϕ of 1, (c) non-uniform Lewis number at L/D of 2 and ϕ of 0.25, (d) non-uniform Lewis number at L/D of 2 and ϕ of 4, (e) non-uniform Lewis number at L/D of 2 and oxidizer temperature of 1800 K, and (f) non-uniform Lewis number of L/D of 6 and ϕ of 1. (For interpretation of the references to color in this figure legend, the reader is referred to the web version of this article.)

uniform Lewis number simulations are quite different from that obtained at unity Lewis number (Fig. 10(b)). In particular non-uniform Lewis numbers yield thicker regions where the mixture fraction is equal to its most reactive value. These results show the importance of both, flow–chemistry coupling and Lewis number in the evolution of the flame.

The effect of fuel/air ratio is similar to that observed in the homogeneous mixture problem. Recall from Table 5 that τ_{chem} for the fuel-lean and rich cases was 3.5e−4 and 8.0e−5 seconds, respectively. The fuel lean vortex ring therefore has minimal heat release and is the last to auto-ignite (Fig. 9(c)). The fuel rich reacting vortex ring (Fig. 9(d)) auto-ignites behind the vortex ring due to entrainment there, but note that the heat release in the fuel rich vortex ring (Fig. 9(d)) is much more intense compared to the stoichiometric case (Fig. 9(a)).

For the higher oxidizer temperature of 1800 K, ignition occurs nearly instantaneously (Fig. 9(e)). This is because τ_{chem} is an order of magnitude smaller at the higher oxidizer temperature (Table 5). Ignition now occurs along the entire interface between fuel and oxidizer and not just behind the ring. As the flame evolves, heat release is mostly in the front of the vortex ring. The resulting products are then shed into the ring wake and therefore no reaction occurs there.

The stroke ratio changes the spatial behavior of the initial ignition, but not the time taken for initial auto-ignition. Recall from Section 1 that the vortex ring of stroke length 6 is identical to the vortex ring of stroke length of 2 until a non-dimensional time of 2. The effect of stroke length is therefore apparent after non-dimensional time of 2. For the fuel/air ratios and oxidizer temperatures considered, the initial auto-ignition occurs at non-

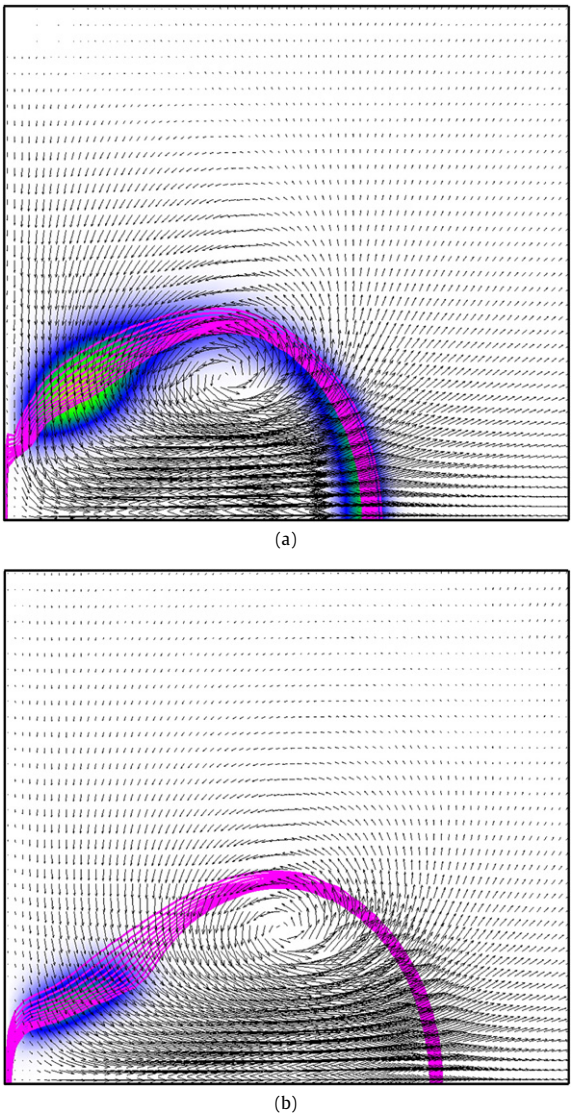

(a) (b)

Fig. 10. Contours of heat release ($\dot{\omega}_n$) and velocity vectors. On each color contour, a contour line is superimposed for ζ. (a) Non-uniform Lewis number (time = 2.25) and (b) unity Lewis number (time = 3.0). (For interpretation of the references to color in this figure legend, the reader is referred to the web version of this article.)

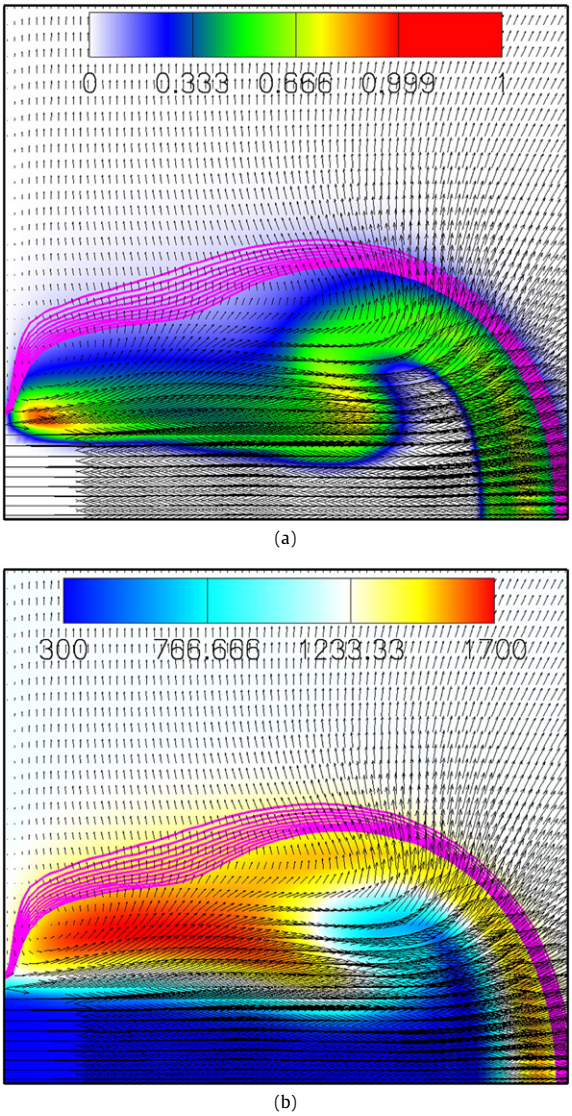

(a) (b)

Fig. 11. Contours of heat release ($\dot{\omega}_n$), temperature (T) and velocity vectors at L/D of 6 (time = 4). On each color contour, a contour line is superimposed for ζ. (a) $\dot{\omega}_n$ and (b) T in Kelvin. (For interpretation of the references to color in this figure legend, the reader is referred to the web version of this article.)

dimensional time ($U_{\text{piston}}t/D$) around 2 as seen in Fig. 10. The fuel that is injected before $U_{\text{piston}}t/D = 2$ therefore auto-ignites in the same manner as the vortex ring with stroke ratio = 2. However fuel that is injected after the $U_{\text{piston}}t/D =$ formation number (approximately 4 [6]) exits the nozzle in a trailing column. As shown in Sau and Mahesh [7] and as visible in Fig. 11(a) the trailing column does not entrain surrounding oxidizer very efficiently. Fuel and oxidizer now mix due to the shear at the edges of the trailing column; auto-ignition therefore occurs in regions of ζ_{MR} there. The flame then propagates toward the vortex ring. Also, note that the expansion associated with heat release in the trailing column forces oxidizer away from the ring (Fig. 11(b)).

4.3. The importance of Lewis number

The temperature field (Fig. 12) may be qualitatively anticipated from the behavior of heat release discussed above. Also, temperature shows the importance of accounting for different rates of diffusion of the different chemical species. Note that for the non-uniform Lewis number simulations, the temperatures are high both in front and rear of the vortex ring. However, when all Lewis numbers are assumed to be unity, temperature rises only behind the vortex ring. The fuel lean vortex ring shows very little temperature rise due to low levels of heat release, and almost behaves like a non-reacting vortex ring. The fuel rich vortex ring on the other hand shows high temperatures. At the higher stroke ratio the temperature rise is along the trailing column. Table 5 lists maximum temperature and burnout time for all simulations. Note that the maximum temperature is higher in the uniform Lewis number flame compared to the non-uniform Lewis number. This behavior has also been observed in axisymmetric simulations of a laminar hydrogen–air jet diffusion flame (Katta et al. [27], Fig. 1 of their paper).

The Lewis number has an interesting effect on the impact of higher oxidizer temperature. The one-step chemistry simulations of Hewett and Madnia [11] and our simulations using the Mueller mechanism at unity Lewis number [28] show that lower oxidizer temperature provides a faster burnout time than the higher oxidizer temperature. This counterintuitive behavior may be explained by noting that at high oxidizer temperature, ignition is nearly instantaneous. The flow immediately expands, which decreases the vorticity, and therefore decreases further mixing. The expansion

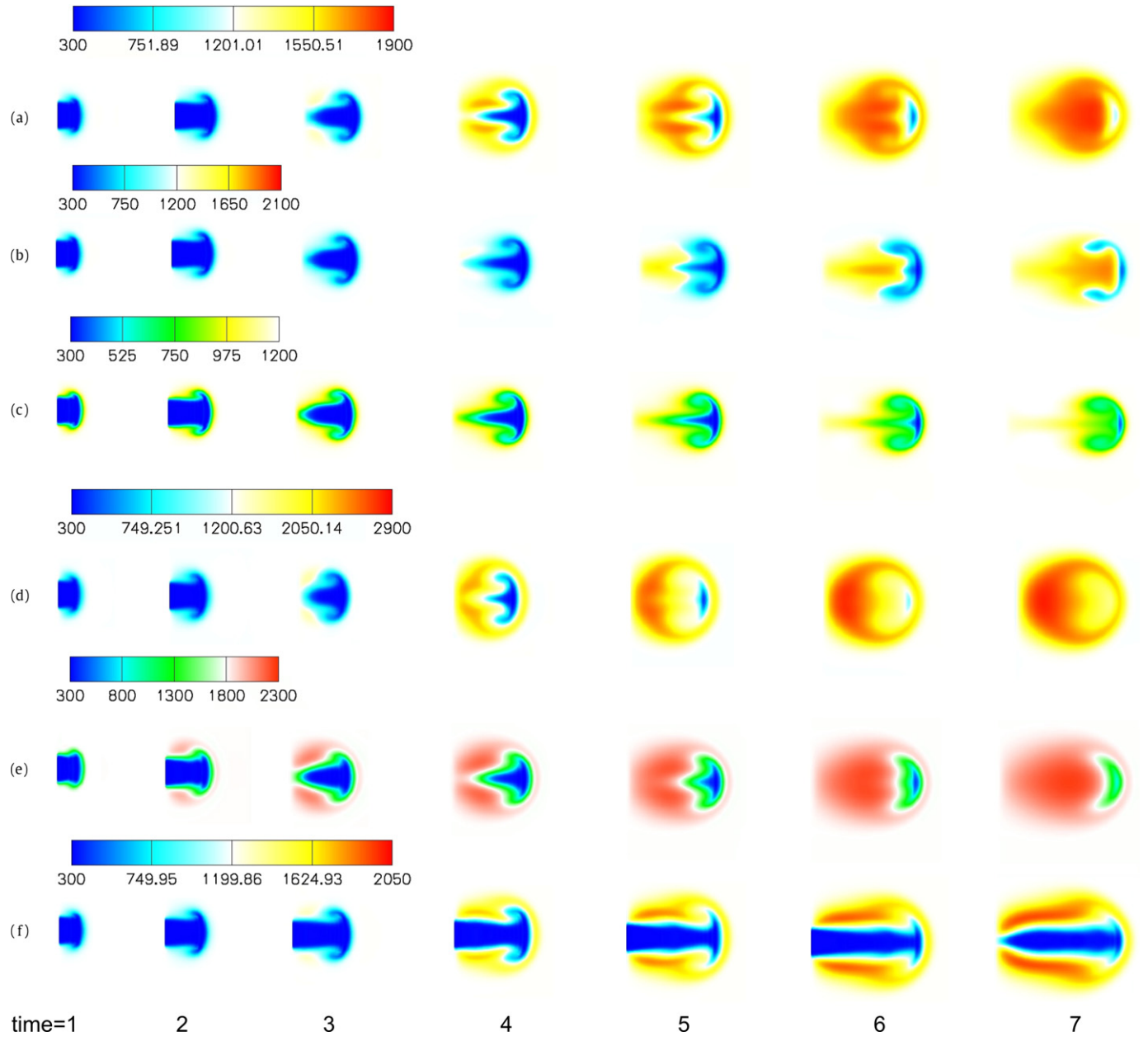

Fig. 12. Time evolution (seven units of time) of temperature (T) in Kelvin. (a) Non-uniform Lewis number at L/D of 2 and ϕ of 1, (b) uniform Lewis number at L/D of 2 and ϕ of 1, (c) non-uniform Lewis number at L/D of 2 and ϕ of 0.25, (d) non-uniform Lewis number at L/D of 2 and ϕ of 4, and (e) non-uniform Lewis number of L/D of 6 and ϕ of 1. (For interpretation of the references to color in this figure legend, the reader is referred to the web version of this article.)

also affects the entrainment of oxidizer. Instead of pushing fresh oxidizer behind the core, oxidizer is pushed into the higher temperature region where there is less fuel. The burnout time is therefore longer.

However, this behavior is an artifact of unity Lewis number. The simulations with non-uniform Lewis number ($Le_k \neq 1$) show that the burnout time is faster in the higher oxidizer temperature flame compared to that at lower oxidizer temperature (Table 5). This behavior may be explained as follows. If the uniform and non-uniform Lewis number flames are compared at the same temperature, ignition time is smaller for the non-uniform Lewis number flame since the fuel diffuses faster toward the oxidizer. Increasing oxidizer temperature decreases ignition time for both cases. However, the relative reduction in ignition time will be less for the non-uniform Lewis number flame since the faster diffusion of the fuel contributes significantly to its lower ignition time.

A general conclusion from Fig. 12 is that each flame has a unique burnout time, maximum temperature and flame shape which cannot be determined by the homogeneous mixture problem, and is a consequence of the coupling between the flow and chemistry.

Fig. 13(c) shows how heat release affects the vorticity of the ring. Note that in the absence of any reaction, the maximum vorticity increases when fluid is being injected and then stays approximately constant until the injection is complete and the injected shear layers roll-up into the vortex ring. After injection, the vorticity decreases steadily due to viscous dissipation. Note that the lean fuel/air ratio ring behaves similarly to a non-reacting vortex ring because it has very little heat release (Fig. 13(c)). The non-uniform Lewis number simulations show the same qualitative trend as the non-reacting ring until the instant (4 time units) when temperature (Fig. 12) reaches the core, at which point the vorticity drops

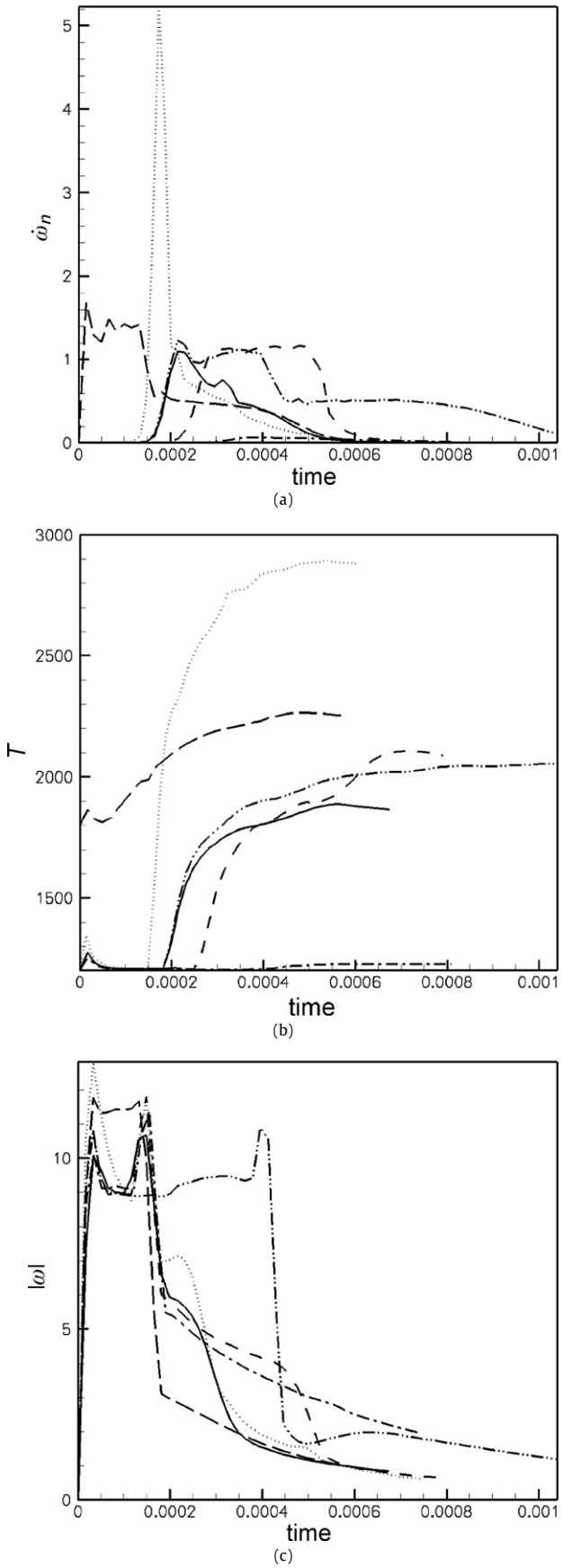

Fig. 13. Maximum value of (a) heat release, (b) temperature in Kelvin (T) and (c) vorticity magnitude versus time in seconds. (—) Non-uniform Lewis number, (– – –) unity Lewis number, (—·—) $\phi = 0.25$, (···) $\phi = 4$, (— — —) oxidizer temperature of 1800 K, (—···—) L/D of 6.

sharply due to core expansion. The uniform Lewis number simulations show a similar trend; the main difference is that the vorticity drops after 6 units of time reflecting the longer ignition delay. At higher oxidizer temperature, heat is released before injection is complete. The initial acceleration of the flow therefore increases the magnitude of vorticity in the injected shear layer at very short times. However once the injection is completed and the ring is formed, the vorticity drops sharply as shown in Fig. 13(c).

5. Summary

This paper uses direct numerical simulation to study the combustion of a vortex ring of hydrogen issuing into hot air. A detailed chemical mechanism from Mueller et al. [13] is used. The simulations use a novel, spatially non-dissipative numerical method developed by Doom et al. [16]. The simulations study the effect of fuel/air ratio, Lewis number, oxidizer temperature and stroke ratio (ratio of piston stroke length to diameter). Also, the well-stirred reactor problem is used as a baseline case to identify the effects of the flow on the auto-ignition and evolution of the flame.

Results show that auto-ignition occurs in fuel lean regions of high temperature and low scalar dissipation at the most reactive mixture fraction (Mastorakos et al. [14]). We also define a most reactive temperature from the homogeneous mixture problem (T_{MR}) and find that while ζ_{MR} does a good job of predicting the onset of ignition, it does not predict the subsequent evolution. T_{MR} is found to predict both the initial ignition and the subsequent evolution for all cases considered.

As Gharib et al. [6] show, coherent vortex rings are obtained for stroke ratios less than the formation number, while a vortex ring followed by a trailing column of vorticity is obtained for stroke ratios greater than the formation number. At moderately high oxidizer temperatures, coherent vortex rings first ignite behind the vortex ring and the heat release then propagates into the core. This is because the ring entrains surrounding oxidizer and sheds mixed fluid in its wake. At higher oxidizer temperatures, ignition occurs instantaneously, along the entire interface between fuel and oxidizer. At stroke ratios greater than the formation number, ignition around the leading vortex rings is different from that in the trailing column. Ignition initially occurs behind the leading vortex ring, and then occurs along the length of the trailing column as more fuel is injected.

The coupling between the flow and chemistry is quite non-trivial even for this simple problem. The Lewis number affects both the initial ignition time as well as the subsequent evolution of the flame. At non-uniform Lewis numbers, faster ignition and burnout times, but lower maximum temperatures are obtained. The Lewis number also affects the location of the initial ignition regions. The influence of higher oxidizer temperature on burnout time is completely different when uniform Lewis numbers are considered. The effect of fuel/air ratio may be anticipated from the homogeneous mixture problem. Higher fuel/air ratios yield higher temperatures and shorter ignition times, while very lean vortex rings behave essentially like non-reacting vortex rings.

Acknowledgments

This work was supported by the AFOSR under grant FA9550-04-1-0341. Computing resources were provided by the Minnesota Supercomputing Institute, the San Diego Supercomputing Center and the National Center for Supercomputing Applications.

References

[1] K. Shariff, A. Leonard, Annu. Rev. Fluid Mech. 24 (1992) 235–279.
[2] T. Maxworthy, J. Fluid Mech. 51 (1972) 15–32.

[3] T. Maxworthy, J. Fluid Mech. 81 (1977) 465–495.
[4] N. Didden, Z. Angew. Mech. 30 (1979) 101–116.
[5] A. Glezer, Phys. Fluids 31 (1988) 3532–3542.
[6] M. Gharib, E. Rambod, K. Shariff, J. Fluid Mech. 360 (1998) 121–140.
[7] R. Sau, K. Mahesh, J. Fluid Mech. 582 (2007) 449–461.
[8] S.L. Chen, J.A. Dahm, Proc. Combust. Inst. (1998) 2579–2586.
[9] S.L. Chen, J.A. Dahm, in: 38th Aerospace Science Meeting and Exhibit, paper AIAA-2000-0433.
[10] S. Chen, W. Dahm, G. Tryggvason, Proc. Combust. Inst. 28 (2000) 515–520.
[11] J.S. Hewett, C.K. Madnia, Phys. Fluids 10 (1998) 189–205.
[12] C. Safta, C.K. Madnia, Combust. Flame 144 (2006) 64–73.
[13] M.A. Mueller, T.J. Kim, R.A. Yetter, F.L. Dryer, Int. J. Chem. Kinet. 31 (1999) 113–125.
[14] E. Mastorakos, T.A. Baritaud, T.J. Poinsot, Combust. Flame 109 (1997) 198–223.
[15] T. Echekki, J.H. Chen, Combust. Flame 134 (2003) 169–191.
[16] J. Doom, Y. Hou, K. Mahesh, J. Comput. Phys. 226 (2007) 1136–1151.
[17] A. Majda, J.A. Sethian, Combust. Sci. Technol. 42 (1985) 185–205.
[18] H.G. Im, J.H. Chen, C.K. Law, Proc. Combust. Inst. 27 (1998) 1047–1056.
[19] T. Colonius, P. Moin, S.K. Lele, Direct Computation of Aerodynamic Sound, Report No. TF-65, Department of Mechanical Engineering, Stanford University, Stanford, CA.
[20] T.S. Cheng, C.Y. Wu, C.P. Chen, Y.H. Chao, T. Yuan, T.S. Leu, Combust. Flame 146 (2006) 268–282.
[21] J.A. Miller, C.T. Bowman, Prog. Energy Combust. Sci. 15 (1989) 287–338.
[22] G.P. Smith, D.M. Golden, M. Frenklach, N.W. Moriarty, B. Eiteneer, M. Goldenberg, C.T. Bowman, R.K. Hanson, S. Song, W.C. Gardiner, V.V. Lissianski, Z. Qin, GRI-Mech homepage, http://www.me.berkeley.edu, 1999.
[23] U. Maas, J. Warnatz, Combust. Flame 74 (1) (1988) 53–69.
[24] M. O'Conaire, H.J. Curran, J.M. Simmie, W.J. Pitz, C.K. Westbrook, Int. J. Chem. Kinet. 36 (2004) 603–622.
[25] R.J. Kee, F.M. Rupley, J.A. Miller, M.E. Coltrin, J.F. Grcar, E. Meeks, H.K. Moffat, A.E. Lutz, G. Dixon-Lewis, M.D. Smooke, J. Warnatz, G.H. Evans, R.S. Larson, R.E. Mitchell, L.R. Petzold, W.C. Reynolds, M. Caracotsios, W.E. Stewart, P. Glarborg, C. Wang, C.L. McLellan, O. Adigun, W.G. Houf, C.P. Chou, S.F. Miller, P. Ho, P.D. Young, D.J. Young, D.W. Hodgson, M.V. Petrova, K.V. Puduppakkam, Chemkin Release 4.1, Reaction Design, San Diego, CA, 2006.
[26] T. Poinsot, D. Veynante, Theoretical and Numerical Combustion, Edwards, 2005.
[27] V.R. Katta, L.P. Goss, W.M. Roquemore, Combust. Flame 94 (1994) 60–74.
[28] J. Doom, K. Mahesh, in: 46th Aerospace Science Meeting and Exhibit, paper AIAA-2008-0508.